

A Large Area Magnetic Spectrometer for the
Study of High Energy Neutrino Interactions

A. Benvenuti, D. Cheng, D. Cline, W. T. Ford, R. Imlay,
T. Y. Ling, A. K. Mann, F. Messing, R. L. Piccioni,
J. Pilcher, D. D. Reeder, C. Rubbia, R. Stefanski and L. Sulak

Department of Physics
Harvard University
Cambridge, Massachusetts 02138

Department of Physics
University of Pennsylvania
Philadelphia, Pennsylvania 19174

Department of Physics
University of Wisconsin
Madison, Wisconsin 53706

Fermilab
P. O. Box 500
Batavia, Illinois 60510

Abstract

We describe the design, construction and performance of a large solid iron magnetic spectrometer which has been used to identify and measure the momentum of muons produced by interactions of neutrinos with nucleons. The resolution of the spectrometer varies from $\Delta p/p = 10\%$ to $\Delta p/p = 50\%$ depending on the momentum of the muon and the characteristics of the optical system used to record the muon trajectory.

A. Design Criteria and Construction

The characteristics of the neutrino beam which influence most strongly the design of a muon spectrometer are:

- i) the extended source of muons produced in ν interactions
- ii) the production of muons at large angles with respect to the beam axis.

These features require a magnet with a large area to maximize the angular acceptance over a source of about $2\text{m} \times 2\text{m} \times 6\text{m}$.

The deflection of a charged particle in a magnetic field can be written:

$$\theta = \frac{\int B \cdot d\ell}{Kp} \approx \frac{B \cdot \ell}{Kp}$$

where B is the magnetic field, ℓ the path length in the field, p is the momentum and K a constant. A fundamental difficulty in using the deflection to infer the momentum is multiple coulomb scattering:

$$\theta_{\text{ms}} = \frac{.014}{p\beta} \sqrt{\ell/L_R}$$

where L_R is the radiation length and p is the momentum in GeV/c . The fractional error of the momentum measurement can then be written

$$\frac{\Delta p}{p} = \frac{\Delta \theta}{\theta} \sim \frac{\theta_{\text{ms}}}{\theta} \propto \frac{1}{B\sqrt{\ell}}$$

The fractional error can be reduced most strongly by increasing the magnetic field, while only slow improvement results from lengthening the trajectory in the field.

By sampling the trajectory at several points within the magnetic field, the effects of significant bremsstrahlung, δ ray production, and pair production can be minimized as discussed below.

The magnet which was constructed is shown in Fig. 1. It was composed of four similar toroids (outer radius 1.83 m, inner radius 0.15 m and length 1.20 m). On each torus are 12 coils equally spaced about the circumference. Each coil has 7 turns of water cooled copper conductor. A magnetomotive force of 84,000 ampere-turns is obtained by imposing a current of 1000 amperes through the 84 turns. This is sufficient to drive the iron well into saturation. The field is circular about the axis and varies from ~ 22 kg near the center to 16.5 kg at the outer periphery. This variation of about 22 per cent is significantly different from the $1/r$ behavior of the magnetic intensity H .

The four modules are mounted on a common structure, separated magnetically from their supports by 2.5 cm of aluminum. The structure and magnet can be moved on commercial transporters.

Five wide gap optical spark chambers each $3\text{m} \times 3\text{m}$ are inserted between the modules. These chambers are viewed by a system of mirrors and lenses such that two stereo views are recorded on a single frame of 70 mm film. The stereo angle is about 15° , scintillation counters are also used to trigger the recording of the event.

B. Calculation and Measurement of the Magnetic Field

The deflection of the muon in the iron is proportional to the magnetic induction \vec{B} in the iron. Since measurements must be made external to the iron we use the boundary conditions to relate our

measurements to \vec{B} in the iron.

Because the available iron was obtainable only in sizes small compared to our module, we were compelled to piece it together. A further restriction was imposed by the lifting capacity of the crane in the building (Lab C) which was 7.5 tons. Thus each module is composed of six pancakes 0.2 m in thickness, and each pancake is further composed of four pieces as shown in Fig. 1. The pieces were flame cut to size and the interior load bearing surfaces were machined. For ease in assembly and in order to introduce field measuring apparatus, 0.25 cm aluminum spacers were placed between the pieces of each pancake creating gaps.

Although the ideal situation would be a single radial gap, we were led by the considerations detailed above to compromise by adapting the existing gaps for the field measurement. Hall probes mounted on fiber glass strips were inserted into the gaps as shown in Fig. 1. The component of the field perpendicular to the gap is equal to the component in the iron, which can easily be related to \vec{B}_θ by the geometry.

Detailed measurements were taken of the field in the gaps of each of the four modules. About half of the pancakes were sampled. Variations of the measurements were less than 2% among the various pancakes.

The field \vec{B} was calculated by numerical integration of the boundary value problem and by an analytical calculation using the magnetic scalar potential. The magnetic permeability was measured in iron samples and the iron is assumed to be homogeneous. Although

the return legs of the coil were initially calculated they made a negligible contribution (less than 0.2%).

The best analytical expression of the field is the simple

$$B_{\theta} = \mu(H)\mu_0 H$$

where

$$H = \frac{I}{5r}$$

and I = ampere turns, r = radius in cm, B is in k gauss, $\mu_0 = 10^{-7}$ and μ is the relative permeability dependent on H .

The effect of the gaps, which is very significant, is that B should be modified by an additional term

$$B = B_0 \frac{1}{\left(1 + \frac{\mu \ell_G}{2\pi r}\right)}$$

where ℓ_G is the length of the gaps.

This equation is iteratively solved since $\mu(H) = \mu\left(\frac{B}{\mu\mu_0}\right)$. The comparison of the calculated field to the measurements is shown in Fig. 2. The agreement is quite satisfactory. All calculational methods are in agreement although only the simple analytic form is used in the fitting program.

D. Radiative Events and Their Effect on Momentum Resolution

Muons in iron can lose significant amounts of energy in three ways: δ ray production, bremsstrahlung and direct pair production. Nuclear interactions of muons have been calculated and can be neglected.

The probability for a muon to lose greater than ten per cent of its energy in one cm of iron for each of the three processes is

plotted in Fig. 3. Delta ray production is the dominant process.

Preliminary calculations indicate that about 1% of muons will lose $\geq 10\%$ of their energy undetected. Chi-squared tests and other criteria will allow detection, rejection and correction of other such events. The ability to sample the trajectory at intervals in the iron is absolutely necessary to achieve rejection of these events.

E. Measurement of the Resolution and Calibration of the Spectrometer

To determine the response of the spectrometer to muons of known energy, a series of measurements were made with a variable energy monoenergetic secondary beam. The arrangement has been described in detail in the accompanying paper.

Unfortunately, there were relatively few muons in the beam resulting in undesirably large statistical error. Furthermore, there was no momentum analysis over a significant portion of the decay path which skews the momentum distribution of the incident beam toward low momentum. This effect is most serious in the measurements made at 100 GeV/c and 125 GeV/c. Another complication occurred because the muons were incident in the mid plane of the spectrometer and thus deflections were observed using the least precise measurements, because of the small angle stereo viewing of the optical spark chambers.

The results of the measurements are shown in Fig. 4, for incident momenta 20, 35, 70, 100 and 125 GeV/c. No evidence of bias is apparent in the measurements.

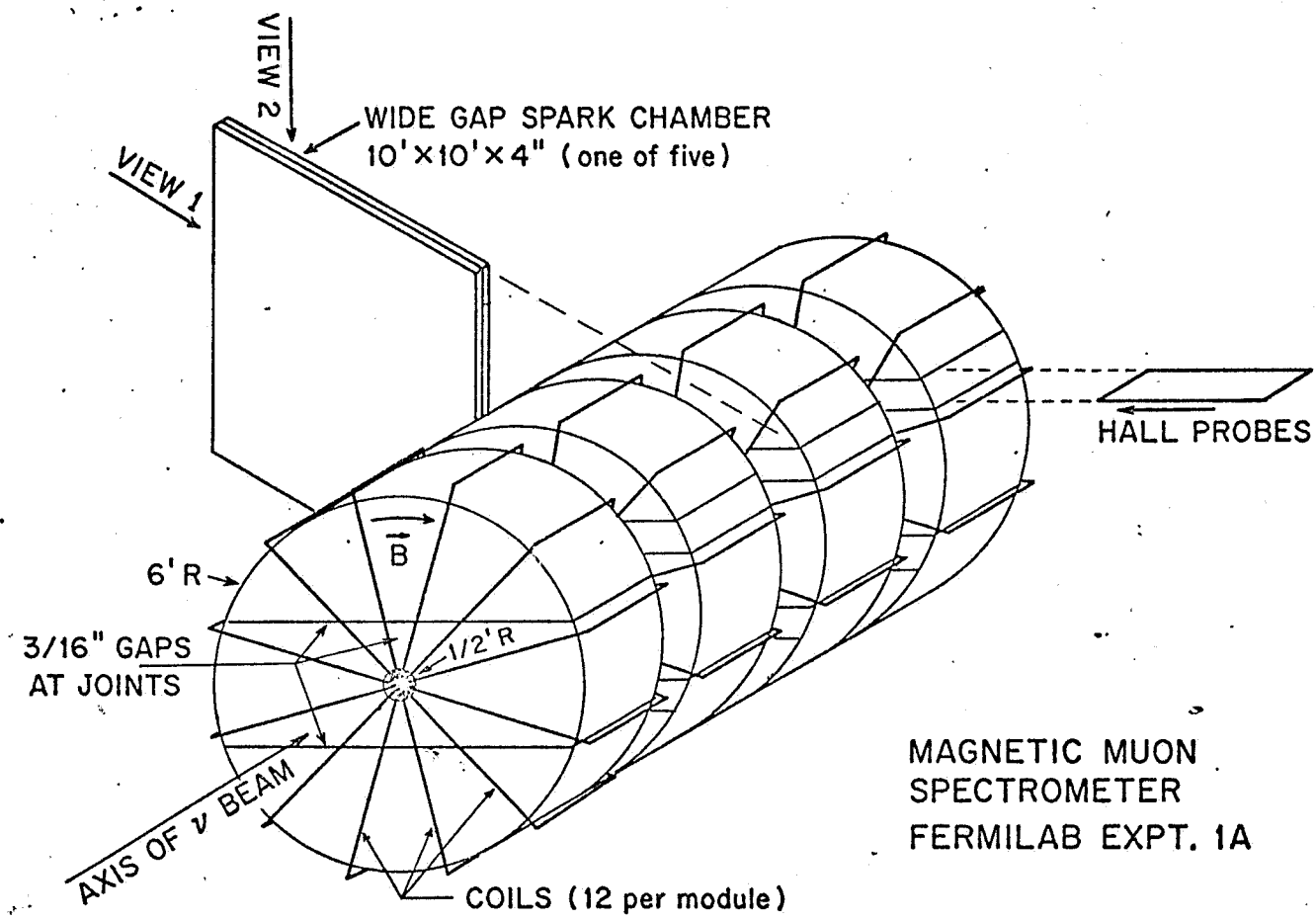
To measure the intrinsic resolution a measurement was made with the current set to zero. These 125 GeV/c trajectories were calculated in the normal manner assuming a non-zero field. The curvature Q/p is plotted in Fig. 5a for these events. The second moment of this distribution is a measure of the error of the "sagitta".

The resolution inferred from this measurement is shown in Fig. 5b. Also shown in Fig. 5b are the estimated resolution in the good stereo plane and that estimated for a uniform azimuthal distribution of muons.

Note the resolution is dominated by multiple scattering below 70 GeV/c, and that to ~ 150 GeV/c errors of $\pm 10\%$ are estimated.

Figure Captions

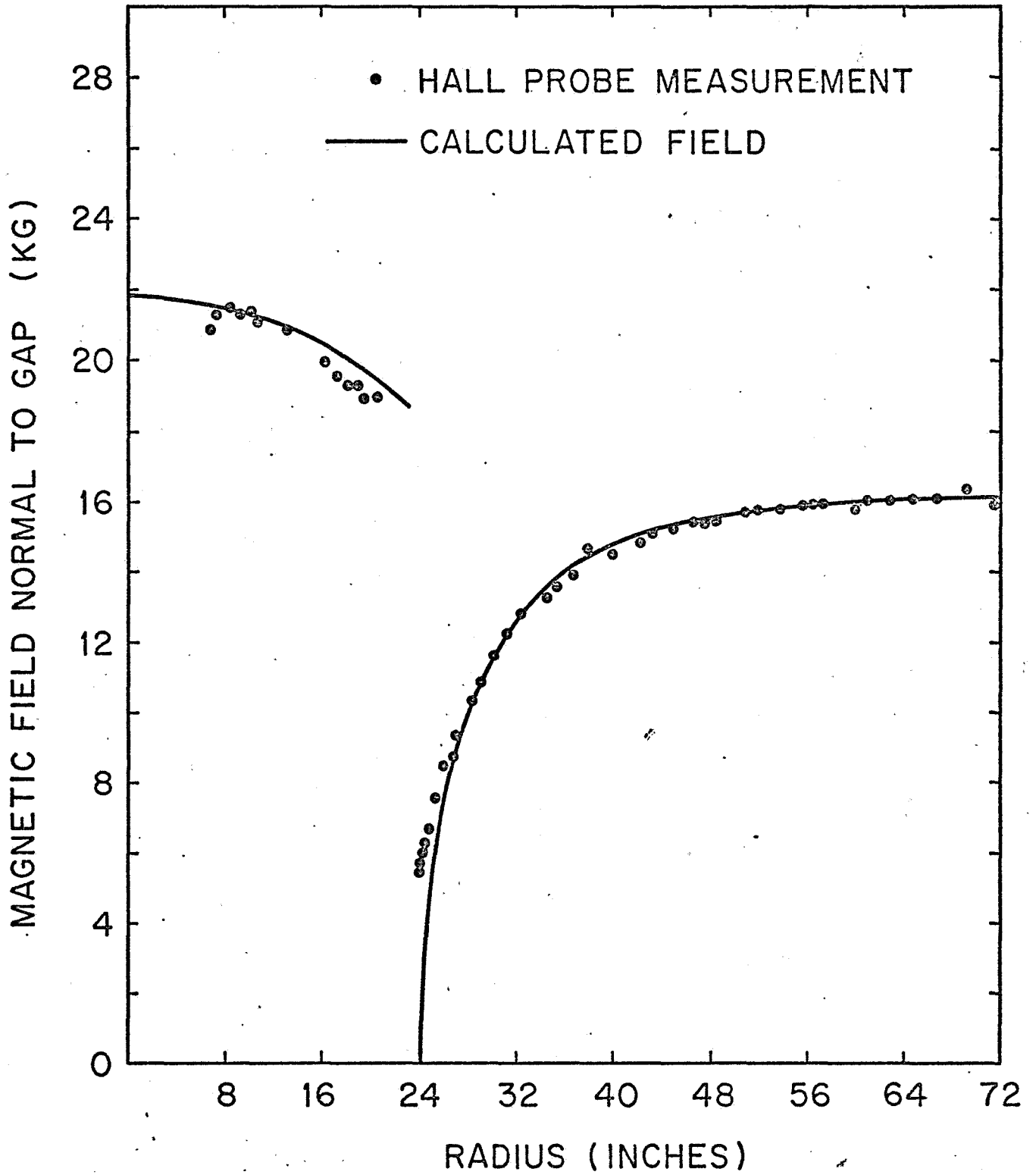
- Fig. 1 Scale drawing of the magnet and associated spark chambers.
- Fig. 2 Magnetic field measurements. Also shown is the field calculated as described in the text.
- Fig. 3 Probability of muon radiating greater than 10% of its energy in a single event per cm in iron. This affects the measurement and thus contributes to the non-Gaussian tails of the distribution of measurements.
- Fig. 4 Calculated momenta for several incident calibration beam momenta.
- Fig. 5 a) Plot of Q/p of tracks taken with current equal to zero but calculated with $I = 800$ amps.
b) Resolution $\Delta p/p$ as a function of momentum.

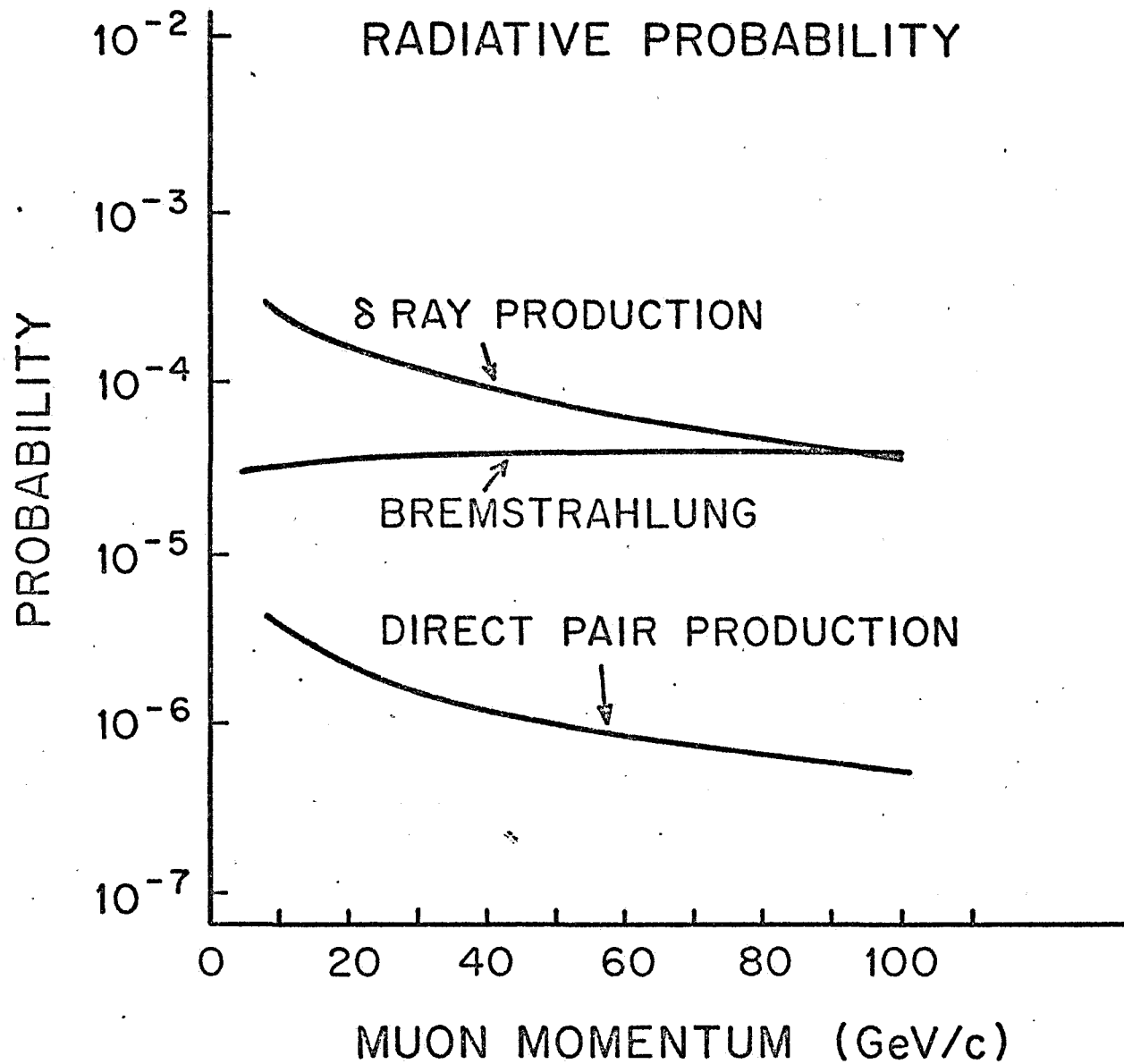


MAGNETIC MUON
SPECTROMETER
FERMILAB EXPT. 1A

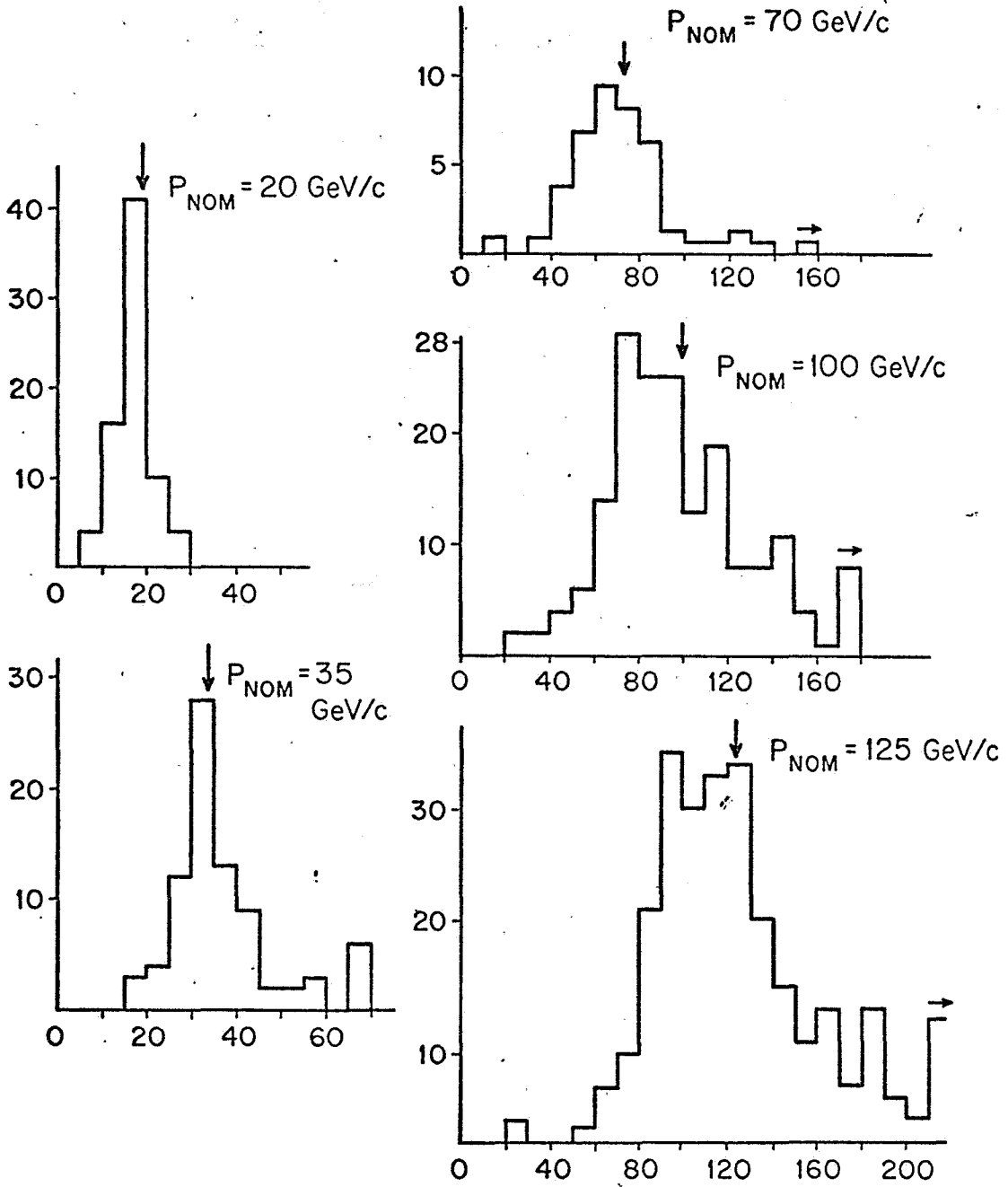
MAGNETIC MUON SPECTROMETER

EXPT. 1A





OBSERVED MUON MOMENTUM SPECTRA OBTAINED
IN CALIBRATION RUNNING FOR EXPT. 1A



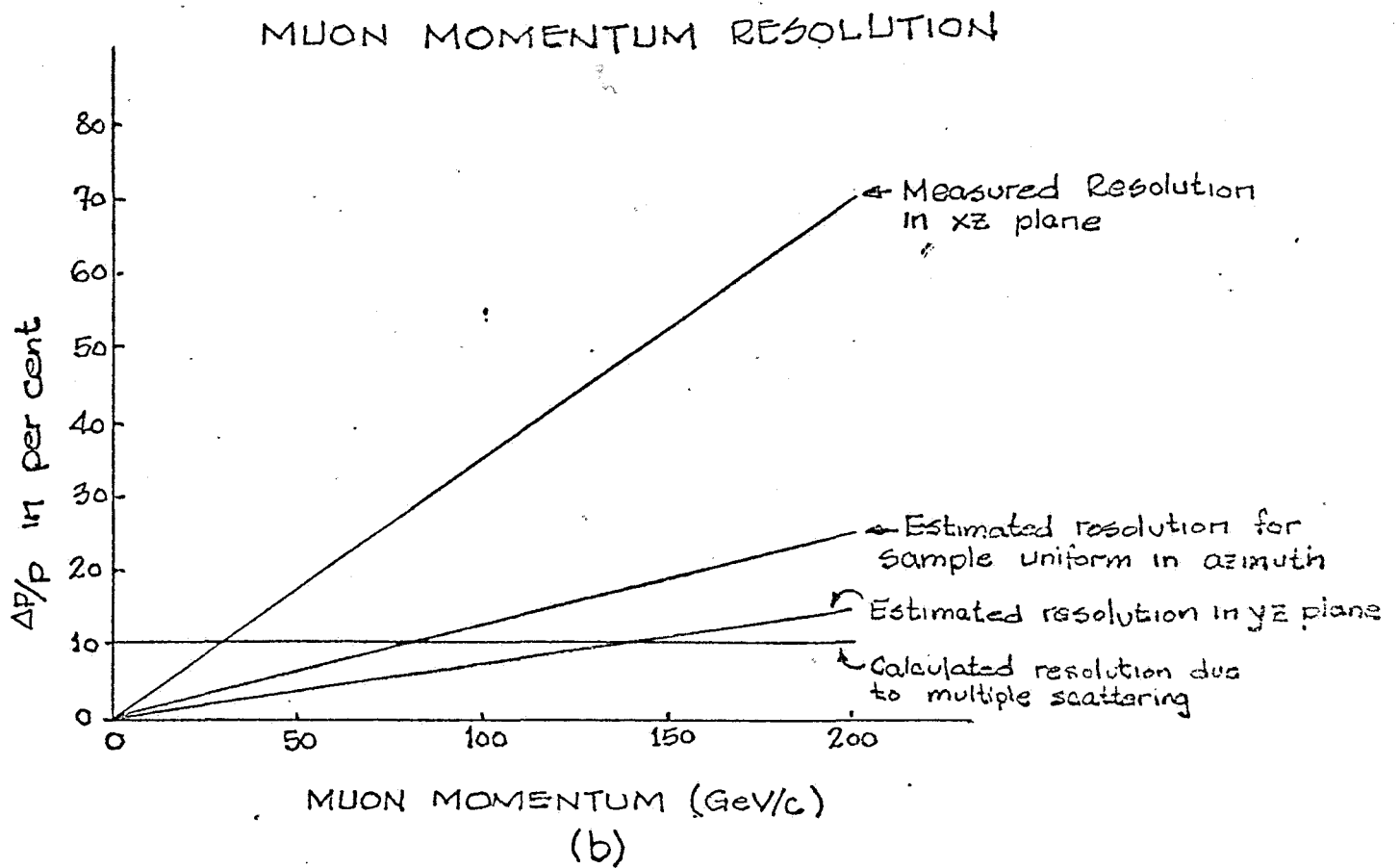
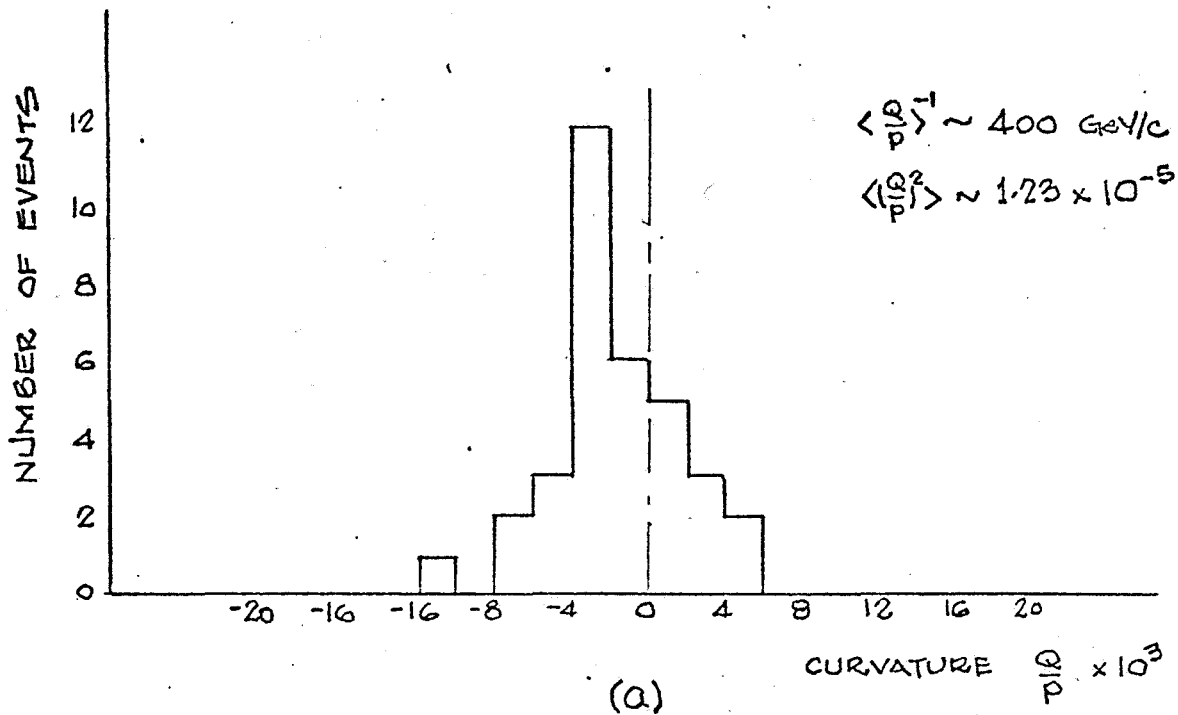


Figure 5